Journal of the Korean Physical Society(Proc. Suppl.), Vol. 28, December 1995, pp. S609~S616

Building a Better World with Buckyballs

David TOMÁNEK
Department of Physics and Astronomy and Center for Fundamental Materials Research
Michigan State University, East Lansing, Michigan 48824-1116, U. S. A.

The C_{60} "buckyball", a prominent member of the recently discovered family of fullerene molecules, is an unusual system with exciting properties. This contribution summarizes the present state of theoretical understanding of the equilibrium structure of carbon clusters, in particular the fullerenes, the optical properties of individual fullerene molecules, superconductivity in the alkali-intercalated C_{60} solid, and the disintegration of fullerenes in collisions and at high temperatures.

I. INTRODUCTION

Until very recently, the only stable bulk forms of elemental carbon have been believed to be graphite and diamond. About ten years ago, this conventional wisdom has been challenged by the discovery of the stable C_{60} molecule with a spherical hollow cage [1]. This molecule, sometimes called "buckyball", turned out to be only a particular representative of the family of "fullerene" molecules, named so for their close resemblance to the geodesic dome structures created by the architect Buckminster Fuller. Later on, it has been found that C_{60} molecules can aggregate to form a molecular crystal. The interest in C_{60} rose dramatically following the successful development of a mass production technique for this system [2].

The resulting research first concentrated on characterizing this molecule and the corresponding solid. Next, spurred by the discovery of superconductivity in the alkali intercalated C_{60} solid [3,4], substantial effort has been invested in modifying the C_{60} molecule and solid, and in the synthesis of other fullerenes. Ongoing research focuses both on the structural and electronic properties of C_{60}-inspired carbon fullerenes. At present, most emphasis is placed on derivatizing and functionalizing pure-carbon fullerenes, investigating more complex spherical or tubular multi-walled structures ("bucky onions" and "bucky tubes") [5,6], synthesising endohedral fullerene complexes containing encapsulated atoms [7], and C_{60} intercalation compounds containing intercalant atoms in the interstitial sites.

In the following, after presenting an overview of theoretical methods, I will address from the point of view of theory several phenomena associated with C_{60} and other fullerenes which make these systems truly promising candidates for a new generation of materials with tailored properties. My main objective is to show that presently available *ab initio* techniques can provide quantitative predictions of these properties. Nevertheless, it appears equally important to isolate the essential physics in each particular problem area and to find good models which generalize the *ab initio* results to other systems.

II. THEORETICAL METHODS

1. Density functional formalism

Perhaps the most powerful *ab initio* technique used in calculations of complex systems – such as modified buckyballs – is the Density Functional Theory (DFT) [8]. It is based on the Kohn-Sham theorem stating that in the ground state, the total electronic energy of a given system is a unique functional of the total charge density $\rho(\vec{r})$. The physical charge density can be obtained by minimizing the functional

$$E[\rho] = T_0[\rho] + \int d\vec{r}\rho(\vec{r})V_{ext}(\vec{r}) + E_H[\rho] + E_{xc}[\rho] = min. \quad (1)$$

Here, T_0 is the kinetic energy functional, $V_{ext}(\vec{r})$ is the potential of the ions, $E_H[\rho]$ is the Hartree and $E_{xc}[\rho]$ is the exchange-correlation functional. The Density Functional technique is parameter-free, and requires only the knowledge of atomic numbers and atomic positions to determine the total energy and the electron density $\rho(\vec{r})$ of a given system. In the Local Density Approximation (LDA), the nonlocal functional $E_{xc}[\rho]$ is replaced by a local function $\tilde{E}_{xc}(\rho)$ which reproduces the exchange-correlation energy in the homogeneous electron gas exactly. Further simplification is achieved by either freezing in the core electrons in their atomic configurations, or by replacing the ionic potentials by first-principles pseudopotentials which combine the nucleus and the core electrons. For clusters, a local Gaussian orbital or a numerical basis can be used. Yet even with these simplifications, *ab initio* DFT calculations are computationally

very intensive. For this reason, many parametrized techniques compete successfully with this formalism.

2. Linear Combination of Atomic Orbitals technique

A computationally efficient way to determine the electronic spectrum and the total energy of large systems is a parametrized Linear Combination of Atomic Orbitals (LCAO) formalism. This one-electron technique provides us with a physically sensible way to extrapolate *ab initio* results to systems with low symmetry. The general expression for the total energy of a carbon cluster is [9,10]

$$E_{tot} = \sum_i E_{coh}(i) \tag{2}$$

$$= \sum_\alpha n_\alpha \epsilon_\alpha + \sum_{i<j} E_r(\{d_{ij}\}) \,. \tag{3}$$

Here, the electronic states of the cluster have been labeled by α and the atomic sites by i, j. The first term in Eq. (3) is the one-electron molecular orbital energy of the cluster, obtained using two-center Slater-Koster [11] matrix elements in the Hamiltonian. The second term describes nuclear and closed-shell repulsion as well as the electronic "overcounting" terms, which are represented by pairwise repulsive energies $E_r(d)$. A recursion technique treatment [10] of the first term in Eq. (3), which describes the nonlocal many-body interactions in the system, leads to linear scaling of computer resources with the number of particles, and parallelizes naturally on massively parallel computer architectures.

The input information consists of the atomic positions and the energy functional parameters for the LCAO Hamiltonian and the repulsive interactions. The information available as output is the total energy of the system E_{tot}, the molecular orbital wave functions, and the energy eigenvalues ϵ_α. The energy functional parameters have been obtained from a fit to LDA results for C_2, carbon chain, graphite and diamond, and are given in Ref. [9]. The computational efficiency of this approach is of particular advantage when computing structural and electronic properties of very large carbon systems, and in molecular dynamics simulations.

3. Molecular dynamics formalism

Molecular dynamics (MD) simulations provide the information about the trajectories of individual atoms, and hence about the time evolution of cluster geometries. More important, they can also be used to determine thermodynamic properties of these systems.

The Lagrangian describing a microcanonical ensemble with a constant number of particles and constant energy can be written as

$$\mathcal{L} = \sum_{i=1}^{N} \frac{1}{2} m_i s^2 \dot{\mathbf{q}}_\mathbf{i}^{\,2} - V(\{\vec{q}_i\}) \,, \tag{4}$$

where $\mathbf{q}_i$ and m_i are the coordinates and the masses of the individual particles, and V is the potential energy of the system.

A canonical ensemble, where the temperature rather than the total energy is constrained, is described by the Nosé-Hoover Lagrangian [12]

$$\mathcal{L} = \sum_{i=1}^{N} \frac{1}{2} m_i s^2 \dot{\mathbf{q}}_\mathbf{i}^{\,2} - V(\{\vec{q}_i\}) + \frac{1}{2} Q \dot{s}^2 - (N_f + 1) T_{eq} \ln s \,, \tag{5}$$

where N_f is the number of degrees of freedom, Q is a constant, and s is a virtual degree of freedom describing the energy flow between the system and the external heat bath, kept at the temperature T_{eq}.

The trajectories of the individual particles are obtained by integrating the equations of motion [13]

$$\frac{d}{dt}\left(\frac{\partial L}{\partial \dot{q}_{i\alpha}}\right) - \left(\frac{\partial L}{\partial q_{i\alpha}}\right) = 0 \,, \tag{6}$$

$$\frac{d}{dt}\left(\frac{\partial L}{\partial \dot{\underline{h}}_{\alpha\beta}}\right) - \left(\frac{\partial L}{\partial \underline{h}_{\alpha\beta}}\right) = 0 \,, \tag{7}$$

$$\frac{d}{dt}\left(\frac{\partial L}{\partial \dot{s}}\right) - \left(\frac{\partial L}{\partial s}\right) = 0 \,. \tag{8}$$

III. APPLICATIONS

In this Section, I will illustrate the usefulness of the above formalism when addressing different phenomena associated with carbon clusters, in particular the C_{60} buckyballs and the C_{60} solid [14]. First, I will discuss the *equilibrium geometry* of small carbon clusters as a function of their size, and the extraordinary stability of fullerenes. These results are crucial for the understanding of the optimum conditions for the synthesis of C_{60}. Next, I will address the *optical properties* of an isolated C_{60} molecule, in particular the possibility of collective electronic excitations. The implied promise in this research is to produce new materials with tailored optical properties. A very interesting property of the intercalated C_{60} solid is its *superconducting behavior* at tens of degrees Kelvin. I will discuss our current understanding of the underlying paring mechanism of electrons. This may lead us to a possible design of novel C_{60} based high-temperature superconductors. Finally, I will discuss the extraordinary stability of the rigid, yet still elastic, fullerenes in *binary collisions*. I will show that cluster fragmentation in inelastic collisions is closely related to *thermally-induced disintegration* of individual fullerenes.

The C_{60} cluster is the most spherical molecule known:

It is a hollow cage with a radius of ≈ 3.5 Å, formed by 60 identically equivalent carbon atoms. The valence charge is delocalized across the surface of the cage, strongly reminiscent of the charge density in a graphite monolayer. This is a consequence of the graphitic sp^2-type bonding in the C_{60} molecule. These strong covalent bonds are responsible for the structural stiffness of this molecule. The C_{60} solid (sometimes called "fullerite"), on the other hand, is a bulk structure obtained by stacking buckyballs. The equilibrium structure at room temperature is a face-centered cubic crystal. The bonding between individual C_{60} molecules is weakly covalent and van der Waals type, very similar to the weak inter-layer bonds in graphite.

1. How do buckyballs grow?

In the following, I will discuss the energetic arguments explaining the abundance of closed-shell fullerene structures, in particular the C_{60} "buckyball", in carbon vapors. The equilibrium structures of carbon clusters at $T = 0$ can be determined efficiently using the LCAO Hamiltonian and the simulated annealing technique [9]. The equilibrium geometries, which were obtained in this procedure, included chains, rings, and hollow fullerene cages. For the sake of comparison, we also considered fullerene caps (fragments of a C_{60} molecule) and graphite flakes.

Our results, shown in Figs. 1(a) and (b), indicate an increasing binding energy per atom with increasing cluster size. Based on these total energy results, which are relevant at $T = 0$, the most stable C_n isomers were found to be chains and rings for $n < 20$. At larger cluster sizes, in particular at $n > 20$, we find rings to be more favorable than chains, since releasing the dangling bond energy of a chain easily offsets the bending energy when forming a ring.

At these larger sizes, however, higher coordinated structures turn out to be energetically much more favorable. For $n > 20$, we find the hollow fullerenes to be the most stable isomers. Also in this size range, the average binding energy per atom is gradually increasing with increasing fullerene size, approaching the value found in a graphene sheet [15]. At sizes exceeding 700 atoms, finally, multi-walled structures are found to be most stable, due to the significance of the attractive interaction between adjacent walls [15].

The C_{60} does not appear to be exceptionally stable. Since in thermodynamic equilibrium the relative abundance of different clusters should reflect their stability, our results would suggest a continuous size distribution of carbon fullerenes in the mass spectra. This is in clear contrast with the observed abundance of the 60-atom structure. We must conclude that simulations beyond these $T = 0$ stability considerations are necessary to explain the abundance of the "magic" C_{60} cluster in the mass spectra.

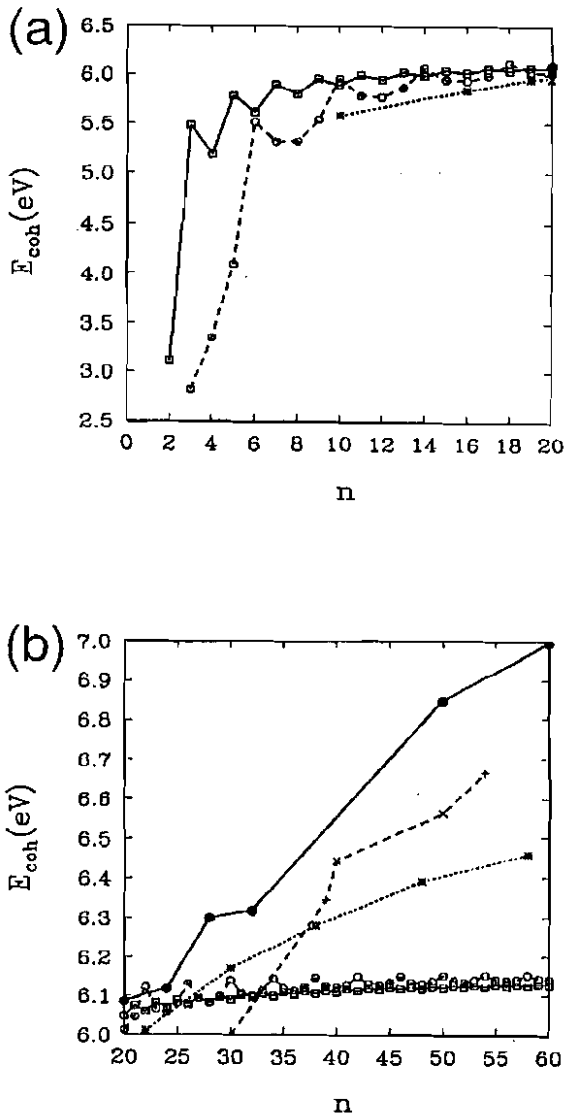

Fig. 1. Binding energy per atom E_{coh} in small carbon clusters as a function of cluster size n, (a) for $n \leq 20$ and (b) for $n \geq 20$. Results for chains (□) are connected by a solid line, results for rings (○) are connected by a dashed line, and results for planar graphite flakes (⋆) are connected by a dotted line. Results for buckled fullerene caps with a pentagonal (×) or a hexagonal basis (+) are connected by a dashed line. Results for hollow fullerene cages (•) are connected by a solid line. (From Ref. [9], ©American Physical Society.)

2. Collective electronic excitations in C_{60} clusters

The structural similarity between a C_{60} molecule and graphite raises the question, whether the optical response of this finite system may have any resemblance with that of macroscopic graphite. In the following, I will review results for the dynamical dipole response of free C_{60} mo-

lecules, published previously in Ref. [16], with emphasis on the discussion of collective plasmon-like excitations.

The optical response of clusters to an external field is described within linear response using the Random Phase Approximation (RPA) [17]. In the present case, the single-particle spectrum is obtained using the parametrized LCAO Hamiltonian discussed previously. The occupied states spread over 19.1 eV, in good agreement with the published LDA value of 18.8 eV [18]. The calculated gap between the highest occupied molecular orbital (HOMO) and the lowest unoccupied molecular orbital (LUMO) is 2.2 eV, larger than the 1.8 eV value which is underestimated in LDA [18]. The "π" states near the HOMO-LUMO gap, and the more strongly bound "σ"states have a similar character as the corresponding states in graphite. The icosahedral symmetry of C_{60} allows us to distinguish singly-, triply-, quadruply- and pentuply-degenerate levels. A large number of optical transitions is allowed by the dipole selection rules.

In the particular case of a dynamical dipole field along the z-direction, which is applied to a spherical molecule such as C_{60}, the calculation can be simplified significantly by anticipating the form of the dipole operator which describes the response of the system. As discussed in Ref. [9], the dipole operator D_z is dominated by two contributions: $D_z^{(1)}$, originating in the intersite charge transfer across the molecule, and $D_z^{(2)}$, stemming from the polarization of individual carbon atoms.

In the free response, which ignores the screening of transitions by electron-hole pair excitations, the lowest dipole-allowed transition is the $HOMO \longrightarrow LUMO+1$ transition which occurs at an energy $\hbar\omega < 3$ eV. In the RPA treatment of dynamical screening, the low-lying transitions are slightly blue shifted and, more important, their oscillator strength is reduced by a factor of typically 10 with respect to the free response. A factor of 400 quenches the $HOMO \longrightarrow LUMO+1$ transition to only an insignificant peak in the spectrum. Even though the calculated spectrum in the frequency range $\hbar\omega < 10$ eV resembles the observed absorption spectrum in a dilute C_{60} solution [19], the integrated oscillator strength in this range remains well below the value of 240 (which is the total number of active electrons), as predicted by the f-sum rule.

The missing oscillator strength is found at higher energies. The oscillator strength, which occurs as a dense featureless spectrum in the free response, piles up to a giant collective excitation at $\hbar\omega \approx 30$ eV in the RPA response calculated with $D_z^{(1)}$ only. The consideration of also $D_z^{(2)}$-induced transitions causes a fragmentation and red shift of this mode into an energy range of $\hbar\omega \approx 20$ eV. This prediction has been subsequently confirmed by the observation of a giant resonance at $\hbar\omega \approx 20$ eV in the photoionization spectrum of C_{60} [20]. Collective excitations at frequencies ranging between $20-30$ eV have also been observed in C_{60} films [21–23].

To investigate the nature of this collective mode, an LDA-RPA calculation was performed for an infinitely thin spherical jellium shell with the radius of C_{60}, carrying 240 conduction electrons [16]. The calculation predicted a single absorption peak at a frequency $\hbar\omega \approx 15-20$ eV, which lies very close to the Mie plasmon frequency $\hbar\omega_{Mie} = \hbar[4\pi\rho e^2/(3m)]^{1/2} \approx 25$ eV of a solid metal sphere with 240 free electrons and the radius of the C_{60} cluster. The origin of the high value of the collective mode frequency is consequently the large valence electron density ρ in the C_{60} molecule. This leads to the conclusion that collective electronic excitations occur in fullerenes as small as the C_{60} molecule. The nature of these modes, which occur at frequencies far beyond the HOMO-LUMO gap, resembles closely that of a classical Mie plasmon.

A more refined calculation of the RPA response of fullerenes to external fields [24], not restricted to the dipole response described by $D_z^{(1)}$ and $D_z^{(2)}$, shows that the excitation spectrum of probably all fullerenes (investigated were C_{20}, C_{60} and C_{70}) is dominated by the above discussed "σ" mode at $\hbar\omega_\sigma \approx 20$ eV and a softer "π" mode at $\hbar\omega_\pi \approx 6$ eV. These two modes have also been observed in electron energy loss spectra of C_{60} fullerite films [23], and appear to be the analogues of the π and σ plasmons in graphite [25]. In graphite, the low-frequency π mode has been interpreted by the in-plane response of the weakly bound p_π system to a field parallel to the layers. The high-frequency σ mode has been assigned to the out-of-plane motion of the strongly bound σ system of s and p electrons in response to a field perpendicular to the layers.

It appears that the finite fullerene molecules show a well-defined signature of plasmon modes which are closely related – in nature and in frequency – to the σ- and π-plasmons of graphite. The large oscillator strength of these modes is collected from lower-lying particle-hole excitations which consequently experience strong dynamical screening.

3. Superconductivity in the alkali doped C_{60} solid

Potentially the most important property of the C_{60} solid is its superconducting behavior when doped with alkali atoms [3,4]. In the following, I will present a quantitative Bardeen-Cooper-Schrieffer (BCS) theory which has been used successfully to describe the superconducting behavior of C_{60} [26]. The electronic states of the alkali doped M_3C_{60} solid are calculated using the LDA and the LCAO formalism discussed above. The vibrational modes of the solid are determined using an extended Keating Hamiltonian which describes both on-ball and inter-ball vibrations.

McMillan's expression for the critical temperature for superconductivity T_c reads [27]

$$T_c = \frac{\hbar\omega_{log}}{1.2\,k_B}\, exp\Big(\frac{-1.04(1+\lambda)}{\lambda-\mu^*-0.62\lambda\mu^*}\Big) \qquad (9)$$

In accordance with other standard superconductors, $\mu^* \approx 0.1$ was used for the effective Coulomb repulsion. The stiff on-ball vibrational modes of C_{60} yield $\frac{\hbar\omega_{log}}{k_B} \approx 1400$ K for the "Debye temperature" of the solid. With the electron-phonon coupling constant $\lambda \approx 0.6$, to be derived below, we can explain the observed value $T_c \approx 30$ K in Rb_3C_{60} [4].

The electron-phonon coupling constant is given by $\lambda = 2N(E_F)V$, where $N(E_F)$ is the electronic density of states at the Fermi level, and V is the Bardeen-Pines interaction which couples two electrons to a Cooper pair. The large value of λ is a consequence of both a large density of states at the Fermi level and a strong coupling of these states to vibrational states.

The conduction band is derived from the t_{1u} lowest unoccupied molecular orbital (LUMO) of C_{60}, and has p_π character. Due to the small inter-ball hopping, the width of this band is small, $W \approx 0.5$ eV [18,28]. For a featureless (e.g. rectangular) band, one can estimate $N(E_F) \approx 6/0.5\ \mathrm{eV}^{-1} \approx 10\ \mathrm{eV}^{-1}$. LDA calculations give $N(E_F) \approx 20\ eV^{-1}$ for a half filled band [18,28]. This density of states is at least one order of magnitude larger than that of intercalated graphite, consistent with the finding that T_c(intercalated graphite) $\ll T_c(M_3C_{60})$.

The vibrational eigenmodes of the crystal were determined using an extended Keating Hamiltonian, with parameters adjusted to reproduce the vibrational spectra of the C_{60} solid. The coupling to the conduction states was investigated for each of these modes. These calculations showed that coupling of the librational modes at $\nu \approx 10\ cm^{-1}$ can be neglected, while inter-ball optical modes at $\nu \approx 100\ cm^{-1}$ couple weakly. The important modes are on-ball modes at a frequency range $\nu \approx 200 - 1600\ cm^{-1}$. Among the most strongly coupling modes are the radial buckling H_g modes at $\nu \approx 400\ cm^{-1}$, the tangential pentagon breathing A_g mode at $\nu \approx 1600\ cm^{-1}$, and tangential optical H_g modes at $\nu \approx 1600\ cm^{-1}$. These modes gave a value of $V \approx 21$ meV per C_{60}. The above determined large values of V and of $N(E_F)$ are responsible for a large electron-phonon coupling constant λ.

The dominant contribution of on-ball modes to the electron-phonon coupling makes it possible to treat electron-phonon coupling in relationship to a dynamical Jahn-Teller effect for the charged C_{60} molecule, and consider solid C_{60} as a molecular crystal [29]. In this case, when changing the alkali intercalant M in M_3C_{60}, λ and consequently also T_c should only depend on the C_{60}-C_{60} separation which modifies $N(E_F)$. One would expect an increase of T_c with increasing lattice constant of M_3C_{60}, which is achieved by substituting a heavier alkali element M [28]. The same argument would lead to the conclusion that a reduction of the lattice constant, due to increasing pressure, should result in a reduction of T_c. Both these effects have been verified experimentally [28].

In conclusion, standard BCS theory was found to be capable of providing a quantitative explanation of superconductivity in the alkali doped C_{60} solid. The observed large value of T_c is linked to the high Debye temperature, a large value of $N(E_F)$, and a strong coupling of on-ball vibrational modes to states at E_F [26,28].

4. Collision dynamics of fullerenes

Next, I will discuss the stability and reactivity of C_n fullerene clusters in binary collisions. Of particular interest in this study was the question of a potential synthesis of more complex structures, such as multi-walled fullerenes (or "bucky onions") [5], by impact-induced encapsulation of the smaller C_{60} buckyball inside the larger C_{240} fullerene. In order to better understand the reaction dynamics, the motion of the individual atoms during the collision process was visualized in a video movie.

Microcanonical molecular dynamics simulations of the collision process were performed at different initial center-of-mass kinetic energies. The C_{60} and the C_{240} clusters were prepared in their equilibrium structures. In the first set of simulations investigating central collisions, the clusters were given an initial linear momentum, zero angular momentum, and the impact parameter was set to zero.

At a low 10 eV center-of-mass kinetic energy, the collision between the C_{240} and the C_{60} clusters could be best characterized as an elastic recoil.

At a ten times higher center-of-mass energy of 100 eV, the C_{240}-C_{60} collision is best described as quasielastic scattering. At the point of impact of C_{60} onto the C_{240} cluster, one can observe a heat- and shock-wave propagating fast within the structure, starting at the point of contact. The C_{240}-C_{60} agglomerate is capable of storing the large surplus energy in a substantial structural deformation and the many vibrational degrees of freedom of the system. In spite of the extreme deformations which even result in a negative Gaussian curvature of the C_{240} cluster, both clusters depart intact, without exchanging any atoms.

Finally, at only three times higher center-of-mass energy of 300 eV, the C_{240}-C_{60} collision leads to an impact-induced fragmentation. The intuitive expectation, that the more rigid C_{60} structure might penetrate the "floppy" wall of the larger C_{240} fullerene, proves to be incorrect. The opposite process occurs — it is the smaller C_{60} cluster which fragments first, leaving the larger C_{240} structure vibrationally highly excited, yet intact. C_{60} is observed to fragment into a structure consisting of linked chains and rings, as well as fragments. A very similar fragmentation dynamics is also observed in simulations assuming a nonzero impact parameter and nonzero initial angular momentum of the fullerenes prior to collision.

The physics underlying this particular fragmentation process is relatively simple. Upon impact, the excessive center-of-mass kinetic energy is distributed into the internal degrees of freedom of both clusters; this vibra-

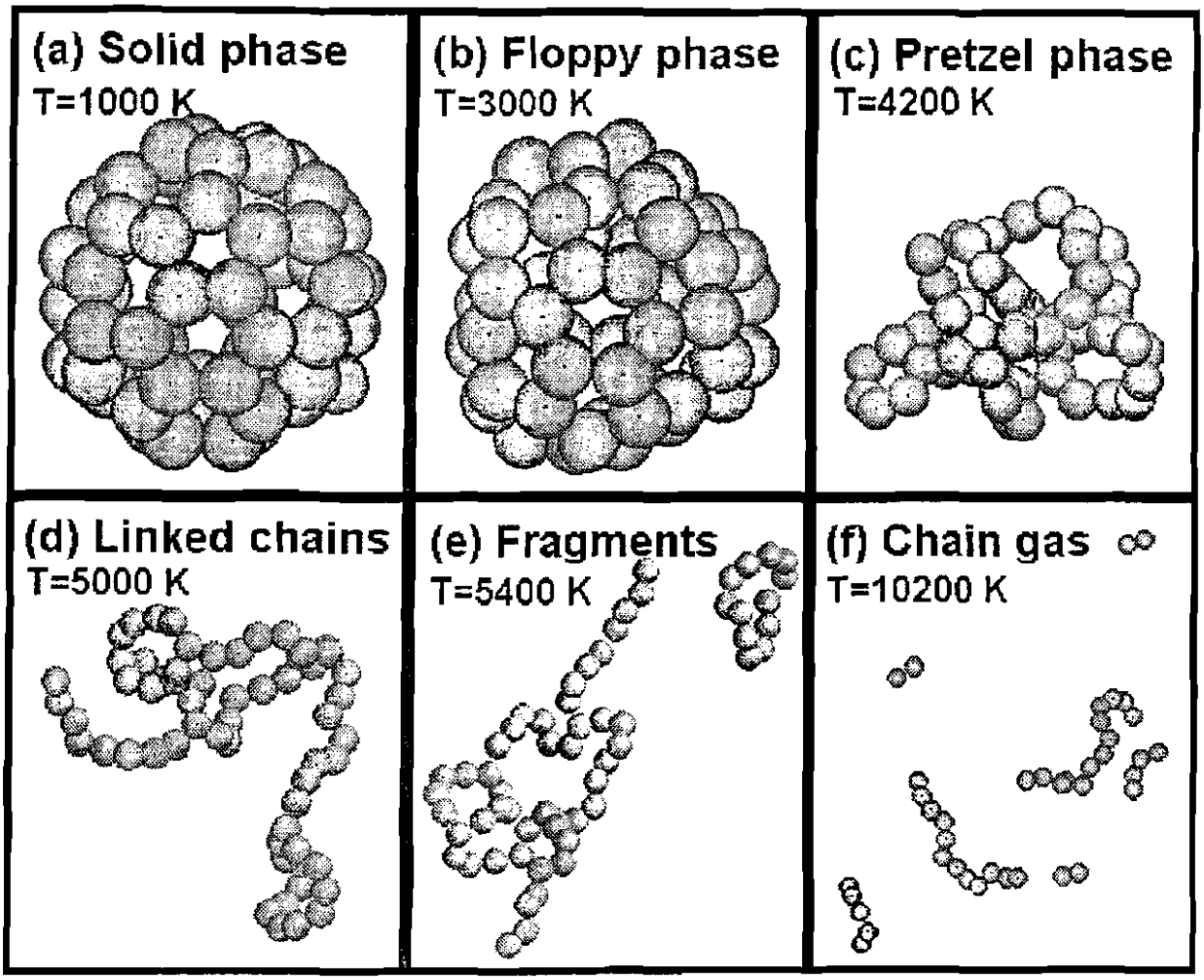

Fig. 2. "Snap shots" illustrating the geometry of a C_{60} cluster at temperatures corresponding to the different "phases" discussed in the text. (From Ref. [30], ©American Physical Society.)

tional energy appears as heat. The fewer degrees of freedom of the smaller C_{60} cluster experience a higher excitation which results in a higher temperature. Due to the limited amount of vibrational energy which can be stored in the anharmonic potentials, the energy surplus is consumed in the heat of "melting" and partly the heat of "evaporation". The structural transformation of the fragmented C_{60} cluster at high temperatures is driven by the vibrational and structural entropy which is obviously much higher for the floppy one-dimensional chain and ring substructures than the more rigid fullerene structure.

If this explanation is correct, the same structure consisting of linked rings and chains should also occur in *isolated* fullerenes which have been exposed to temperatures beyond those causing melting. As will be shown in the following Subsection, this is indeed the case. More important, this establishes an intriguing link between the impact- and thermally-induced fragmentation of clusters.

5. How do buckyballs melt?

The present study, originally inspired by the surprising results of above described inelastic collisions, is intended to answer some fundamental questions related to the nature of thermally induced structural transformations in fullerenes and finite clusters in general. The first important question is, whether atomic clusters – such as fullerenes – undergo *"phase transitions"* such as melting, and what the *"phase diagram"* would look like. Next, one would like to know how to best *characterize* these "phases". Finally, one would like to understand the *driving force* for such "phase transitions".

These and some other related questions have been addressed in a Nosé-Hoover molecular dynamics simulation of the melting and evaporation process of three prototype fullerenes, namely C_{20}, C_{60}, and C_{240}. The details of the simulation are discussed in Ref. [30]. The results

presented below complement nicely those of recent microcanonical ensemble simulations on C_{60} and C_{70} [31].

The key result of the simulation is the total energy of an isolated fullerene as a function of heat bath temperature. In the temperature range of interest, namely between 1,000 K and 10,000 K, the energy E shows a generally linear increase with temperature. The specific heat $c_V = dE/dT$ is generally close to the classical value $c_V = 3k_B$/particle. Strong peaks in the specific heat occur close to 3,000 K and 4,000 K. The peaks get more pronounced with increasing size of the system and, since they are reproducible, can be viewed as a signature of a phase transition which, rigorously speaking, should only occur in an infinite system. Even though the "phase transitions" are gradual in finite systems, the concept of "phases", separated by reproducible features in the specific heat, appears to be useful.

Perhaps the most straight-forward characterization of these "phases" can be achieved by capturing the atomic motion on a video movie, or at least by visualizing "snap shots" of the MD simulation, as shown in Fig. 2. Fig. 2(a) shows that the C_{60} molecule keeps its structure at least up to $T = 1,000$ K. After the first "phase transition" just below $T = 3,000$ K, the systems gets "floppy", as shown in Fig. 2(b). At times, C-C bonds break open in this "phase", and rings of carbon atoms open like a valve. Such processes are always reversible; all atoms "know" their equilibrium positions. Beyond the "melting temperature" of $T_M \approx 4,000$ K, the system transforms to a "pretzel" consisting of linked rings, as shown in Fig. 2(c). Experimental evidence for such a transition has recently been obtained from diffusion experiments [32,33]. At a temperature exceeding 5,000 K, the rings break open, yielding a structure composed of linked chains, shown in Fig. 2(d). As shown in Figs. 2(e) and (f), the continuous structure of this aggregate eventually breaks into smaller fragments. From this point on, the simulations describe a system of chain and ring fragments rather than the thermodynamics of C_{60}.

More meaningful for the characterization of the different "phases" than mere visualization of "snap shots" is the (time-averaged) binding energy distribution in the system, based on the energy decomposition of Eq. (2). This appears to be more meaningful than a discussion of changing coordination numbers which are ill-defined in amorphous systems.

Below the "melting temperature" $T_M \approx 4,000$ K, all atoms are essentially equivalent and their binding energy is characterized by a single peak in the distribution near 7 eV. This peak broadens and shifts to lower values with increasing temperature. In the "pretzel phase", the binding energy distribution changes drastically to a bi-modal distribution which describes the occurrence of two inequivalent types of sites: the twofold coordinated atoms in the strained rings and the more stable multiply-coordinated atoms at the links of these rings. The onset of the "linked chains phase" is marked by a third peak near a binding energy of ≈ 5 eV associated with chain ends. At even higher temperatures, the spectrum broadens and the average stability of the structure decreases.

A simple estimate of the "melting transition" from fullerenes to pretzels can be obtained by comparing the free energies of the two structures which must be equal at the melting point. At this temperature, the larger entropy must outweigh the lower stability of the pretzel structure. The Nosé-Hoover simulations contain the information about the heat uptake, and hence the entropy associated with the atomic degrees of freedom (structural, vibrational and rotational entropy). A comparison between the entropy of a fullerene and a linear chain (with equal numbers of atoms) indicates a nearly constant entropy difference $\Delta S \approx 2k_B$ (per atom) between these structures [34]. The binding energy difference (per atom) between a fullerene and a chain of ≈ 1 eV leads, together with the above value for the entropy difference, to an estimated "melting temperature" of fullerenes near 5,800 K. This value is of the same order of magnitude as the value obtained in the MD simulation, and also close to the melting point of graphite, T_M(graphite) = 3,823 K [35]. These results confirm that the "melting transition" in fullerenes at $T_M \approx 4,000$ K is driven mainly by the vibrational and structural entropy.

IV. SUMMARY AND CONCLUSIONS

I have discussed successful application of both *ab initio* and parametrized techniques to quantitative calculations of the *stability* and *electronic properties* of carbon clusters, in particular carbon fullerenes and related systems. Theoretical results indicate that

- At $T = 0$, the *equilibrium shapes* of free C_n clusters are chains and rings for $n < 20$, spherical fullerene cages for $n > 20$, and multi-walled onions for $n >$ 700 atoms. Entropy is expected to play a significant role at $T > 0$.
- The *optical response of fullerenes* is dominated by collective excitations at $\hbar\omega_\pi \approx 6$ eV and $\hbar\omega_\sigma \approx 20$ eV with counterparts in the π and σ plasmons of graphite.
- *Superconductivity* in the alkali doped C_{60} solid can be explained by the standard BCS theory. The important factors responsible for a large critical temperature T_c are a large electronic density of states at E_F and efficient coupling of conduction electrons by stiff on-ball modes.
- The threshold for *inelastic C_{240}-C_{60} collisions* is at $E_{CM} \approx 200$ eV. The smaller cluster "melts" upon impact.
- Upon heating, free fullerenes show a *structural transformation* to "pretzels" at $T \approx 4,000$ K, which is driven by vibrational and structural entropy.

ACKNOWLEDGEMENT

This work has been performed in collaboration with (alphabetically) George Bertsch, Aurel Bulgac, Richard Enbody, Seong Gon Kim, Michael Schlüter, Yang Wang, and Weiqing Zhong, whose contributions are gratefully acknowledged. Financial support has been provided by the National Science Foundation under Grant No. PHY-8920927, the Air Force Office of Scientific Research under Grant No. F49620-92-J-0523DEF, and by the sponsors of the 1995 conference in Taejon, Korea.

REFERENCES

[1] H. W. Kroto, J. R. Heath, S. C. O'Brien, R. F. Curl, and R. E. Smalley, Nature **318**, 162 (1985).
[2] W. Krätschmer, L. D. Lamb, K. Fostiropoulos, and D. R. Huffman, Nature **347**, 354 (1990).
[3] A. F. Hebard, M. J. Rosseinsky, R. C. Haddon, D. W. Murphy, S. H. Glarum, T. T. M. Palstra, A. P. Ramirez, and A. R. Kortan, Nature **350**, 600 (1991).
[4] M. J. Rosseinsky, A. P. Clarum, D. W. Murphy, R. C. Haddon, A. F. Hebard, T. T. M. Palstra, A. R. Kortan, S. M. Zahurak, and A. V. Makhija, Phys. Rev. Lett. **66**, 2830 (1991).
[5] Daniel Ugarte, Nature **359**, 707 (1992).
[6] Sumio Iijima, Nature **354**, 56 (1991); Sumio Iijima, Toshinari Ichihashi, and Yoshinori Ando, Nature **356**, 776 (1992).
[7] J. R. Heath, S. C. O'Brien, Q. Zhang, Y. Liu, R. F. Curl, H. W. Kroto, and R. E. Smalley, J. Am. Chem. Soc. **107**, 7779 (1985).
[8] P. Hohenberg and W. Kohn, Phys. Rev. **136**, B864 (1964); W. Kohn and L. J. Sham, Phys. Rev. **140**, A1113 (1965).
[9] D. Tománek and Michael A. Schlüter, Phys. Rev. Lett. **67**, 2331 (1991).
[10] W. Zhong, D. Tománek and George F. Bertsch, Solid State Commun. **86**, 607 (1993).
[11] J. C. Slater and G. F. Koster, Phys. Rev. **94**, 1498 (1954).
[12] W. G. Hoover, Phys. Rev. **A31**, 1695 (1985); S Nosé, Mol. Phys. **52**, 255 (1984).
[13] M. P. Allen and D. J. Tildesley, *Computer Simulation of Liquids* (Oxford, New York, 1990).
[14] Synthesis and topology of large fullerenes has been reviewed by Robert F. Curl and Richard E. Smalley in Scientific American, October 1991, p. 54.
[15] D. Tománek, W. Zhong, and E. Krastev, Phys. Rev. **B48**, 15461 (1993).
[16] G. F. Bertsch, A. Bulgac, D. Tománek and Y. Wang, Phys. Rev. Lett. **67**, 2690 (1991).
[17] G. D. Mahan, *Many-Particle Physics*, (Plenum Press, New York, 1981).
[18] Susumu Saito and Atsushi Oshiyama, Phys. Rev. Lett. **66**, 2637 (1991).
[19] H. Ajie, M. M. Alvarez, S. J. Anz, R. D. Beck, F. Diederich, K. Fostiropoulos, D. R. Huffman, W. Kratschmer, Y. Rubin, K. E. Schriver, D. Sensharma, and R. L. Whetten, J. Phys. Chem. **94**, 8630 (1990).
[20] I. V. Hertel, H. Steger, J. de Vries, B. Weisser, C. Menzel, B. Kamke and W. Kamke, Phys. Rev. Lett. **68**, 784 (1992).
[21] J. H. Weaver, J. L. Martins, T. Komeda, Y. Chen, T. R. Ohno, G. H. Kroll, N. Troullier, R. E. Haufler and R. E. Smalley, Phys. Rev. Lett. **66**, 1741 (1991).
[22] Yahachi Saito, Hisanori Shinohara, and Akinori Ohshita, Japan. J. Appl. Phys. **30**, L1068 (1991); G. Gensterblum, J. J. Pireaux, P. Thiry, R. Caudano, J. P. Vigneron, Ph. Lambin, A. A. Lucas and W. Krätschmer, Phys. Rev. Lett. **67**, 2171 (1991).
[23] G. Gensterblum, J. J. Pireaux, P. Thiry, R. Caudano, J. P. Vigneron, P. Lambin and A. A. Lucas, Phys. Rev. Lett. **67**, 2171 (1991).
[24] A. Bulgac and N. Ju, Phys. Rev. **B46**, 4297 (1992); Nengjiu Ju, Aurel Bulgac and John W. Keller, Phys. Rev. **B48**, 9071 (1993).
[25] K. Zeppenfeld, Z. Phys. **211**, 391 (1968); K. Zeppenfeld, Z. Phys. **243**, 229 (1971); H. H. Venghaus, Phys. Stat. Sol. (b) **71**, 609 (1975); R. Klucker, M. Skibowski and W. Steinmann, *ibid*, **65**, 703 (1974); U. Büchner, *ibid*, **81**, 227 (1977); U. Diebold, A. Preisinger, P. Schattsdchneider and P. Varga, Surf. Sci. **197**, 430 (1988).
[26] M. Schluter, M. Lannoo, M. Needels, G. A. Baraff, and D. Tománek, Phys. Rev. Lett. **68**, 526 (1992).
[27] W. L. McMillan, Phys. Rev. **167**, 331 (1968).
[28] M. Schlüter, M. Lannoo, M. Needels, G. A. Baraff, and D. Tománek, J. Phys. Chem. Solids **53**, 1473 (1992).
[29] M. Lannoo, G. A. Baraff, M. Schlüter, and D. Tománek, Phys. Rev. **B44**, 12106 (1991).
[30] Seong Gon Kim and David Tománek, Phys. Rev. Lett. **72**, 2418 (1994).
[31] Eunja Kim, Young Hee Lee and Jae Young Lee, Phys. Rev. **B48**, 18230 (1993).
[32] J. M. Hunter, J. L. Fye, E. J. Roskamp, M. F. Jarrold, J. Phys. Chem. **98**, 1810 (1994).
[33] G. von Helden, N. Gotts, and M. T. Bowers, Nature **363**, 60 (1993).
[34] This is true below the "melting point"; both structures are very similar and hence have the same entropy above the "melting point".
[35] *CRC Handbook of Chemistry and Physics*, 62th edition (CRC Press, Boca Raton, Florida, 1990) p. B-10.